



OPEN

Production of $\text{Ni}_{0.5}\text{Co}_{0.5}\text{Fe}_2\text{O}_4$ /activated carbon@chitosan magnetic nanobiocomposite as a novel adsorbent of methylene blue in aqueous solutions

Zakaria Dastoom

Methylene blue is a cationic dye, not degraded naturally due to its aromatic rings. Accordingly, biological, chemical, and physical water treatment methods have been proposed for its removal. Adsorption is an economical and effective method in this regard. In this study, the nickel–cobalt ferrite/activated carbon@chitosan magnetic nanobiocomposite was synthesized as an adsorbent. The nano-adsorbent was evaluated with FESEM, which estimated the particle size at ~16.64 nm. According to EDAX analysis, the purity of particles was 99%. XRD characterization showed the successful coverage of chitosan, correct placement of nickel–cobalt ferrite, and the nono-structure of crystallites. The specific surface area was 316 m²/g using the BET theory and 285 m²/g using the Langmuir theory, and the porosity volume was 0.18 cm³/g. According to the VSM analysis, magnetic reluctance and coercive force were 1.1 emu/g and 499 Oe, respectively. The FTIR analysis showed that the reaction was successful, and methylene blue was present on the adsorbent surface. The methylene blue adsorption test indicated that 388 mg/g of the dye was adsorbed (97% dye removal), and the final concentration reached 6 mg/L after 8 h. The point of zero charge (pHpzc) was 6.8.

Improper disposal of pollutants such as heavy metal ions, dyes, pharmaceutical effluents, pesticides, and organic compounds in aquatic environments is a global challenge¹. Dyes are pollutants that can cause mutagenesis and carcinogenesis. They are used as base chemicals in various industries such as leather, paper, textile, rubber, plastic, drug, and cosmetics¹. Disposal of dye-containing effluent into water sources increases water pollution, blocks the sunlight, and disturbs the ecological balance². In addition, aromatic rings in the structure of some anionic and cationic dyes turn them toxic and result in dizziness, jaundice, cyanosis, burning, allergy, vomiting, and diarrhea if degraded in the body². As a result, the removal of these pollutants from water is necessary. As technology develops, new methods have been introduced for water treatment. Water treatment methods are divided into three groups: chemical, including oxidation³, ion exchange⁴, and precipitation⁵; physical, including filtration⁶, adsorption⁷, air flotation⁸, and coagulation⁹; and biological, including aerobic and anaerobic². In general, due to the adsorption's low cost and high efficiency, it is the most proper and effective water treatment method. Various compounds have been used as an adsorbent, e.g., carbon nanotubes¹⁰, activated carbon¹¹, zeolite¹², metal oxides¹³, chitosan¹⁴, core–shell nanomaterials¹⁵, magnetic nanocomposites¹⁶, silicone¹⁷, and bilayer hydroxides¹⁸. Among magnetic composites, cobalt ferrite/montmorillonite¹⁹ and graphene oxide/chitosan²⁰ were evaluated for the removal of methylene blue. However, most of these compounds lack porous structure, high chemical stability, biological structure, and easy isolation properties at a time. For example, chitosan cannot be isolated easily. This study aims to synthesize $\text{Ni}_{0.5}\text{Co}_{0.5}\text{Fe}_2\text{O}_4$ /Activated carbon@Chitosan as a nanobiocomposite with all favorable features of a nano-adsorbent. Activated carbon has a porous structure and is a bio-friendly and chemically stable compound that was used in this nano-adsorbent. In addition, chitosan is a natural polymeric adsorbent able to adsorb dyes due to the hydroxyl and amine groups in its polymeric chains²¹. Chitosan was used for its biological properties, preventing dispersion of nanobiocomposite in water, proper reaction with dyes, and improving the adsorption process. Finally, nickel–cobalt ferrite was used to provide the magnetic separation of nanocomposite from aqueous solutions. BET analysis was performed for evaluating porosity, FESEM for confirming the intended morphology, XRD for confirming the crystallization properties and evaluating the crystallites

Shahid Beheshti High School, Toyserkan, Hamedan Province, Iran. email: zakaryadastom@gmail.com

size, FTIR for confirming the reaction success and the presence of methylene blue after adsorption of the dye by the nanocomposite, VSM for evaluating the nanoparticles magnetic properties, and EDAX for assessing the compound purity. The methylene blue adsorption test was performed to optimize parameters effective on the adsorption process, such as adsorption dose, methylene blue initial concentration, pH, and temperature. PHpzc was also obtained to evaluate the effect of pH on the adsorption process in terms of surface charge.

Materials and methods

Materials. $\text{FeCl}_3 \cdot 6\text{H}_2\text{O}$, $\text{CoCl}_2 \cdot 6\text{H}_2\text{O}$, $\text{NiCl}_2 \cdot 6\text{H}_2\text{O}$, $\text{FeCl}_2 \cdot 4\text{H}_2\text{O}$, and NaOH were purchased from the Merck Company, and chitosan from the Sigma Company. In this study, we used activated carbon made in Tuyserkan, Iran, and deionized water.

Synthesis of $\text{Ni}_{0.5}\text{Co}_{0.5}\text{Fe}_2\text{O}_4/\text{AC}/\text{Ch}$ magnetic nanobiocomposite. A homogenous solution of iron salt was made by adding 0.6 g of $\text{FeCl}_2 \cdot 4\text{H}_2\text{O}$ and 1.2 g of $\text{FeCl}_3 \cdot 6\text{H}_2\text{O}$ to 100 mL of deionized water. Then 0.45 g of $\text{NiCl}_2 \cdot 6\text{H}_2\text{O}$ and 0.45 g $\text{CoCl}_2 \cdot 6\text{H}_2\text{O}$ were added to the reaction container and left until homogenization. After a sufficient period, 1 g of activated carbon was added to the container and the solution was stirred for 30 min. Then, 100 mL of 1 M sodium hydroxide was dropped for 1 h to terminate the reaction. The obtained powder was extracted by an external field and dried at 100 °C for 24 h. Finally, the product was functionalized with 1 g of chitosan.

Characterization. We evaluated the microstructure, morphology, and chemical compound of the nanocomposite with a Field Emission Scanning Electron Microscope with Energy Dispersive X-Ray Spectroscopy (FE-SEM- EDAX) (Zeiss Sigma 300). The X-Ray Diffraction (XRD) patterns at angles $2\theta = 10\text{--}80$ were used to identify the crystallography of the nanoparticle using a copper filter. We evaluated the bonding of the nanobiocomposite and confirmed the adsorption of methylene blue on the nanocomposite surface using Fourier transform infrared spectroscopy (FT-IR) with a Rayleigh-WQF-10 instrument in the range of 450–4000 cm^{-1} . The adsorption and desorption isotherm and the specific surface area were also investigated using the Brunauer–Emmett–Teller (BET) and Langmuir theories.

Adsorption test. To evaluate the effect of time on the process of dye absorption by nanoabsorbent, 250 mL of methylene blue with a concentration of 200 mg/liter was prepared and divided into four solutions, one solution was used as a control and 0.1 g of nanoabsorbent was added to each of the other solutions. UV–VIS spectra of three solutions were prepared after 2, 4 and 8 h and the final concentration of the solution was calculated after 8 h. The amount of removal after eight hours was obtained from Eq. (1):

$$R = \frac{(C_0 - C_t) * 100}{C_0} \quad (1)$$

In the above equation, where C_t and C_0 are the initial concentration and the concentration at time t , respectively, in mg/L. The amount of dye absorbed by the adsorbent is obtained from Eq. (2):

$$q_e = \frac{(C_t - C_0) * m}{V} \quad (2)$$

where C_t , C_0 are respectively the initial concentration and concentration at time t in mg/liter, m is the mass of adsorbent in grams and V is the solution volume in liters.

Results and discussion

Characterization of the magnetic nanobiocomposite. *FTIR spectrum of nanobiocomposite before and after adsorption of methylene blue.* The FTIR spectrum of the nano adsorbent before and after the adsorption process is shown in Fig. 1a,b, respectively, and the methylene blue spectrum is shown in Fig. 1c²². The FTIR spectrum of magnetic nanobiocomposite $\text{Ni}_{0.5}\text{Co}_{0.5}\text{Fe}_2\text{O}_4/\text{AC}/\text{Ch}$ was studied at 450–4000 cm^{-1} before methylene blue absorption. The peaks were seen at 3426 cm^{-1} , 2920 cm^{-1} , 1603 cm^{-1} , 1384 cm^{-1} , 1025 cm^{-1} , 821 cm^{-1} , 604 cm^{-1} . The peak of 3426 cm^{-1} was due to the stretching vibration of O–H and N–H bonds in the chitosan²³. The peaks 2920 cm^{-1} and 1384 cm^{-1} pertained to the stretching vibration of C–H in the CH₂, CH, and CHOH bonds, respectively^{16,24}. The peak 1603 cm^{-1} occurred due to the stretching vibration of C=O in the NH=C=O chain²⁵. The present peak at 1025 cm^{-1} indicates the asymmetric stretching of the C–O–C bond²⁶. The peak 821 cm^{-1} was due to the bending vibration of C=C and the peak 604 cm^{-1} pertained to the stretching vibration of Ni–O, Fe–O, and Co–O in the tetrahedral or octahedral inverse spinel structure. by checking Fig. 1b,c and comparing the spectrum of methylene blue and nanoabsorbent after adsorption process, we understand that the peak of nanoabsorbent spectrum at 3442 cm^{-1} is related to OH absorbed in water or N–H in methylene blue, Because the peak is wider compared to the state before methylene blue absorption and is more related to the 3427 cm^{-1} peak in pure methylene blue spectrum. The intense peak of 1578 cm^{-1} is related to the stretching vibration of the C=O bond. The intense peak of 1426 cm^{-1} is related to C–H stretching vibration in bonds such as CH₃ in methylene blue because it is more intense than the peak related to C–H stretching vibration. The peak at 1114 cm^{-1} corresponds to the C–N bond in methylene blue. The rest of the peaks in Fig. 1(c) are also related to the nanobiocomposite structure, the three mentioned peaks 1578 cm^{-1} , 1426 cm^{-1} , 1114 cm^{-1} well confirm the presence of methylene blue after the absorption process on the surface of the nanobiocomposite.

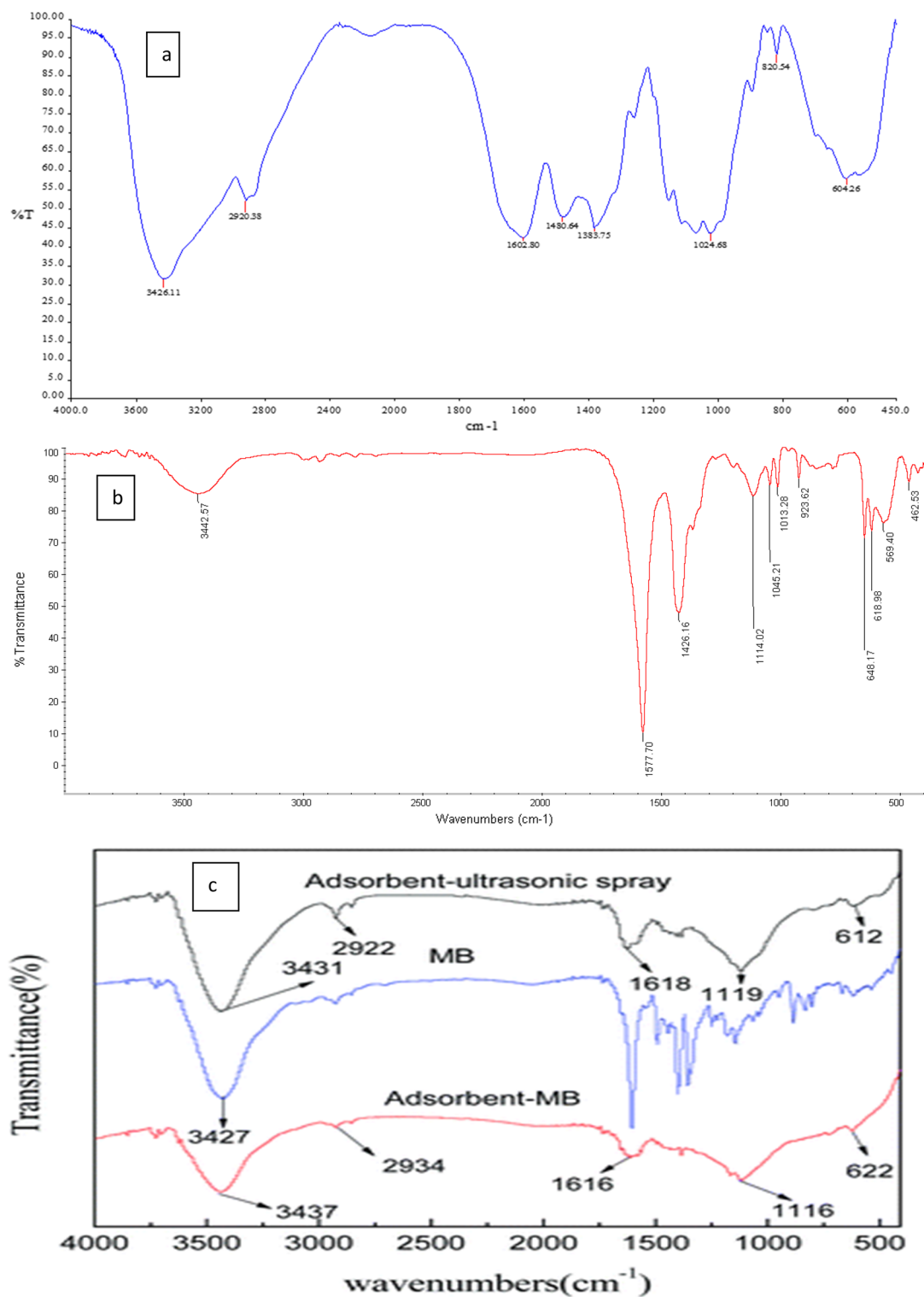


Figure 1. The FT-IR spectrum of the $\text{Ni}_{0.5}\text{Co}_{0.5}\text{Fe}_2\text{O}_4@\text{AC}/\text{Ch}$ nanobiocomposite (a) Before adsorption (b) after adsorption (c) The FT-IR spectrum of the Methylene blue²².

FESEM and element EDAX analyses of the magnetic nanobiocomposite. Figure 2 represents the FESEM of the magnetic nanobiocomposite at 100, 200, 1000, and 10,000 nm magnifications. According to these images, the particle sizes are about 16.64 nm, and the ferrite nickel–cobalt particles are present as small bulks on the activated carbon surface. Element EDAX analysis is shown in Fig. 3, according to which, the ratios of Fe, Co, Ni, C, and O are consistent with the used ratios, indicating the high purity of 99% of the nanobiocompo-site. These two analyzes show the effect of the use of stabilizers and the quality of the raw materials.

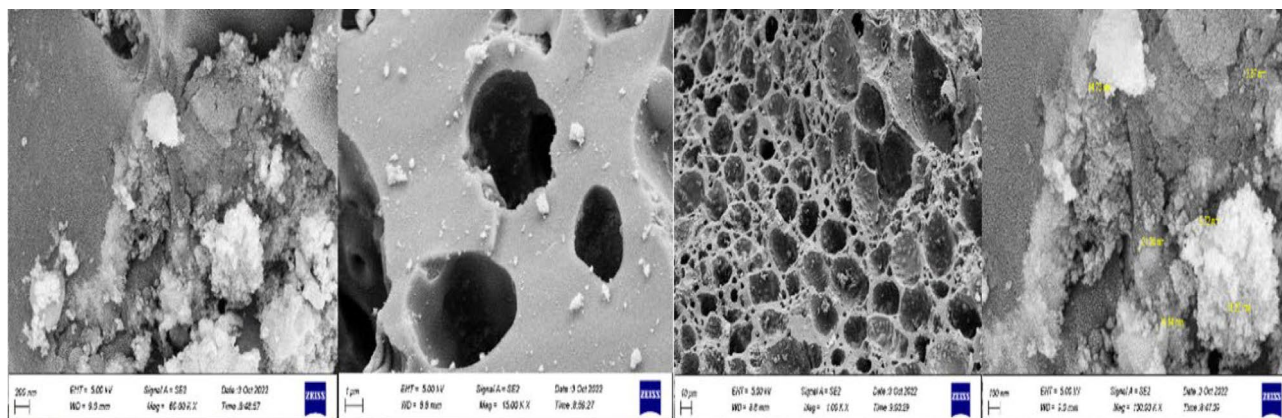


Figure 2. FESEM of the $\text{Ni}_{0.5}\text{Co}_{0.5}\text{Fe}_2\text{O}_4@\text{AC}/\text{Ch}$ magnetic nanobiocomposite.

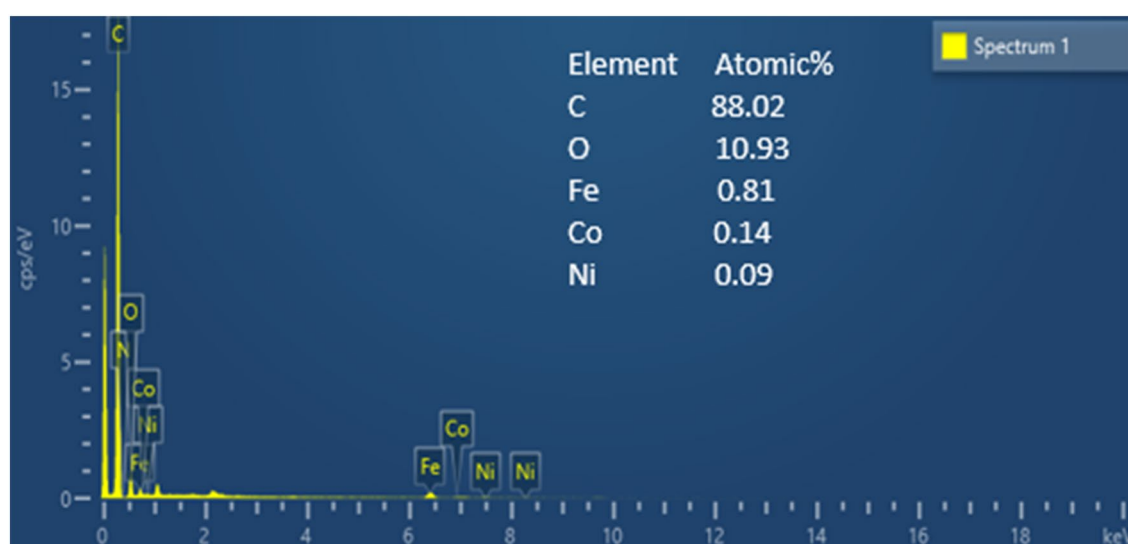


Figure 3. Elemental EDAX analysis of the $\text{Ni}_{0.5}\text{Co}_{0.5}\text{Fe}_2\text{O}_4@\text{AC}/\text{Ch}$ magnetic nanobiocomposite.

Magnetic properties of the nanobiocomposite. Figure 4 represents the magnetization curve of $\text{Ni}_{0.5}\text{Co}_{0.5}\text{Fe}_2\text{O}_4@\text{AC}/\text{Ch}$. According to this curve, the compound is a ferromagnetic nanoadsorbent with a coercive force (H_c) of 499 Oe and saturation magnetization (M_s) of 1.1 emu/g. These values indicate the efficiency of magnetic separation of the nanoadsorbent. As shown in Fig. 4, the nanoadsorbent was homogeneously dispersed in the aqueous solution and easily desorbed after applying an external field. Since this nanobiocomposite uses the magnetic separation method, it is cost-effective and reduces the time of separation.

X-ray diffraction (XRD) patterns of the magnetic nanobiocomposite. The X-ray diffraction patterns of $\text{Ni}_{0.5}\text{Co}_{0.5}\text{Fe}_2\text{O}_4@\text{AC}/\text{Ch}$ are shown in Fig. 5. Peaks were observed at 2θ of 30.3° (220), 35.6° (311), 43.2° (400), 57.26° (511), 62.68° (440), and 74.4° (533). These peaks indicate the cubic spinel structure of ferrite nickel–cobalt, and their similarity with the patterns of Chitosan, Fe_3O_4 , and Co_3O_4 shows that the present study is consistent with the research literature. The size of crystallites was estimated at 96 nm using XPert High-Score Plus software. In the X-ray diffraction pattern of $\text{Ni}_{0.5}\text{Co}_{0.5}\text{Fe}_2\text{O}_4/\text{AC}$, the peaks were observed at about 18.42° , 27.46° , 30.14° , 31.7° , 32.3° , 33.48° , 35.48° , 37.88° , 45.52° , 57.16° , and 62.68° . A comparison of these two diffraction patterns shows that adding chitosan resulted in the filling of inter-crystal planes in the nanocomposite, severely reduced the peaks, and inclined them to higher degrees. Also, the peaks indicate the proper placement of nickel–cobalt ferrite.

BET analysis of the magnetic nanobiocomposite. The BET surface area was obtained using the adsorption/desorption diagram in Fig. 6. The BET equation was used to calculate the volume of the adsorbed monolayer, from which the surface area of the adsorbent is calculated³. The surface area of $\text{Ni}_{0.5}\text{Co}_{0.5}\text{Fe}_2\text{O}_4$ nanobiocomposite /AC@Ch based on Brunner-Emmett-Thaler theory, the value of $316.23 \text{ m}^2/\text{g}$ was obtained from Eq. (3):

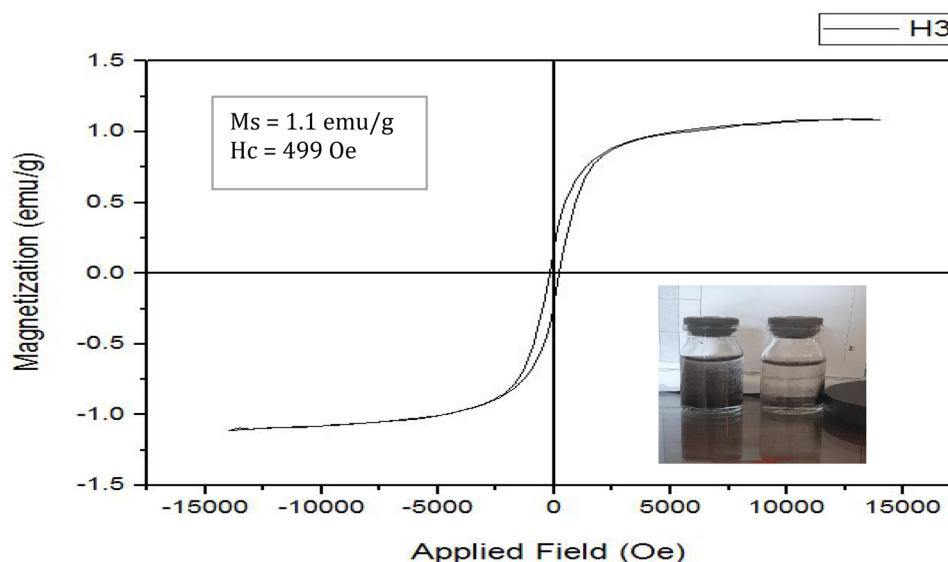


Figure 4. The magnetization curve (VSM) of the $\text{Ni}_{0.5}\text{Co}_{0.5}\text{Fe}_2\text{O}_4/\text{AC}/\text{Ch}$ nanobiocomposite and its easy desorption from aqueous solutions by an external field.

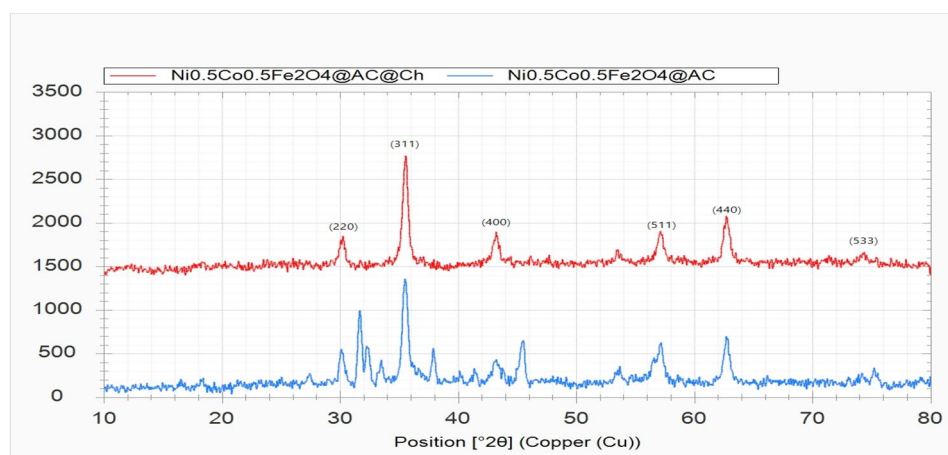


Figure 5. Comparison of X-ray diffraction patterns of $\text{Ni}_{0.5}\text{Co}_{0.5}\text{Fe}_2\text{O}_4/\text{AC}$ and $\text{Ni}_{0.5}\text{Co}_{0.5}\text{Fe}_2\text{O}_4/\text{AC}/\text{Ch}$.

$$S = \frac{V_m N_A}{22400 m} \quad (3)$$

where S is the surface area of the material, N_A is Avogadro's number, m is the mass of the tested sample in grams, 22,400 is the volume occupied by one mole of absorbed gas in the standard state, and V_m is the volume of absorbed gas, which is obtained from Eq. (4):

$$V_m = \frac{1}{A + 1} \quad (4)$$

In the equation above, V_m is the volume of absorbed gas, A is the slope of the BET diagram, the value of the specific surface through Langmuir's theorem based on five assumptions that include ((1) a completely homogeneous surface and there is no priority between molecular adsorption sites. (2) Each adsorption site has only one absorb the molecule and always a single layer of molecules are adsorbed on the surface. (3) The absorption mechanism is the same on the surface of all molecules. (4) There is no interaction between gas molecules. (5) Speed absorption and desorption are equal.) is established, with a value of $286.55 \text{ m}^2 \text{ g}^{-1}$. Both of these theories confirm the use of this material as a suitable surface adsorbent by showing a high specific surface value. The total defect volume was also $0.18 \text{ cm}^3/\text{g}$ ($p/p_0 = 0.990$), which is a relatively high value. The adsorption isotherms are

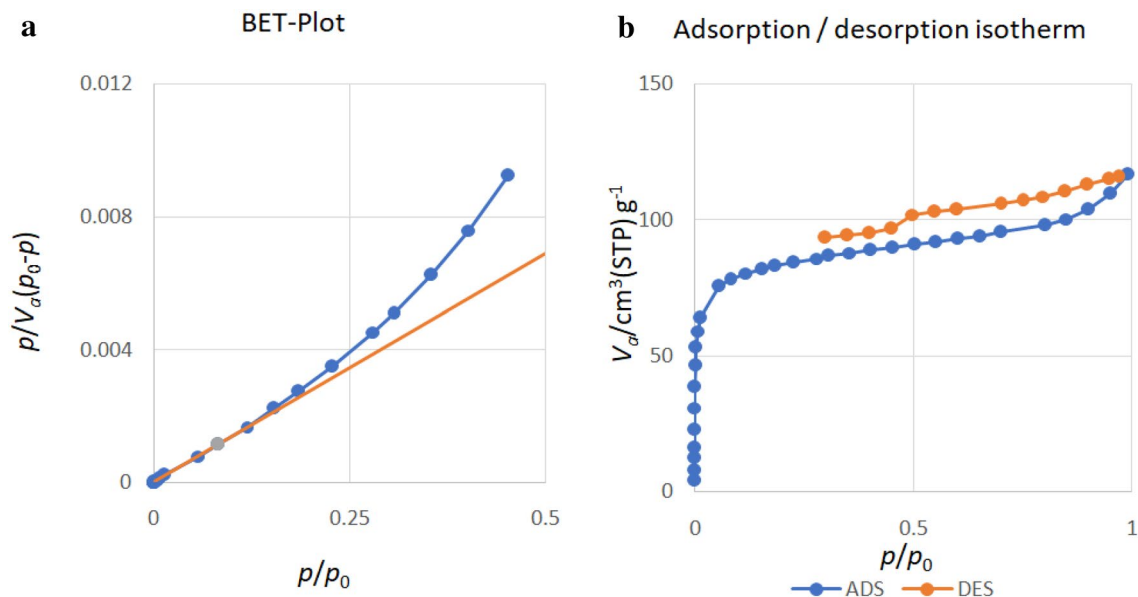


Figure 6. (a) The magnetic nanobiocomposite adsorption/desorption curve, (b) the magnetic nanobiocomposite BET curve.

classified based on the strength of the interaction between the sample surface and the adsorbent surface and the existence or absence of pores. The nanobiocomposite adsorption isotherm was of type IV which is characteristic of mesoporous material. In addition, the adsorption/desorption hysteresis in the diagram shows the conical geometry of the pores. Table 1 represents the comparison between the surface area of adsorbents in previous literature and the present study. As shown in this table, the specific surface of $\text{Ni}_{0.5}\text{Co}_{0.5}\text{Fe}_2\text{O}_4/\text{AC@Ch}$ is higher than most organic and non-organic composites. The relatively larger specific surface areas and total pore volumes of the magnetic nanobiocomposite confirm its dye removal capability.

PHpzc. The value of PHpzc was obtained by solid addition method of 6.8. That is, at a pH less than 6.8 bar, the adsorbent surface is positive and at a pH greater than 6.8 bar, the adsorbent surface is negative. Given that we know that methylene blue is a cationic dye, it is natural that its absorption rate is not as high as that of anionic dyes. Because at a lower pH of 6.8, methylene blue and the adsorbent both have a positive charge, so they repel each other, so in this condition, the absorption rate of methylene blue is lower than that of anionic dyes. But at pH higher than 6.8, the absorption rate of methylene blue is not high compared to the ideal case of anionic dyes, because in this case the number of OH^- increases. However, the adsorbent was able to absorb a good amount of methylene blue. The diagram of ΔPH -initial pH of magnetic nanobiocomposite is shown in Fig. 7.

The effect of time on the absorption process. UV-Vis spectra of the Methylene blue solutions at stop time 2, 4, 8 and the control sample is shown in Fig. 8a and Comparison of the control sample and the absorbed sample after 8 h is shown in Fig. 8b. As shown in Fig. 8a, with time, the amount of adsorbed dye increases because the depth of the peaks is less than that of the control sample. And as shown in Fig. 8b, finally after 8 h, the maximum amount of dye is absorbed, which is the final concentration of the solution is 6 mg/L, the amount of dye absorbed after 8 h is $q_8 = 388 \text{ mg/g}$ and the amount of color removal was determined to be 97%.

Adsorbent	S_{BET} (m^2/g)	References
$\text{Ni}_{0.5}\text{Co}_{0.5}\text{Fe}_2\text{O}_4/\text{AC@Ch}$	316.23	This study
$\text{CoFe}_2\text{O}_4/\text{AC@Ch}$	474.36	26
$\text{Fe}_3\text{O}_4/\text{SiO}_2$ Core-Shell	300.80	15
Activated carbon/ NiFe_2O_4	157.10	27
Fe_3O_4 -GS	62.43	28
CTS-MNPs	112	29
Cs-m-GMCNTs	39.20	21
CoFe_2O_4 -chit	2	1

Table 1. Comparison of the adsorbents surface area (S_{BET}) in pervious literature and the present study.

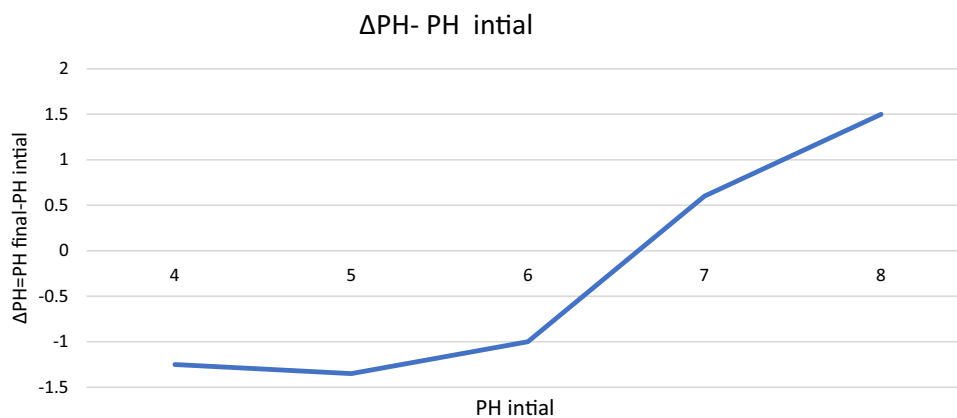


Figure 7. Δ PH- PH initial diagram of magnetic nanobiocomposite.

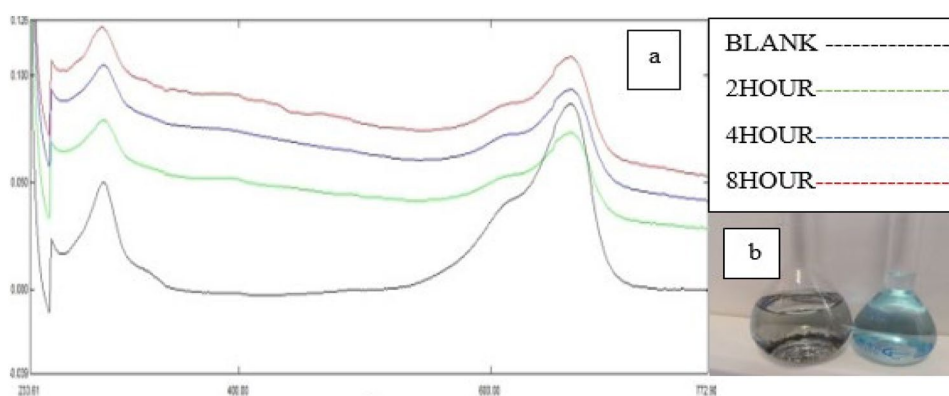


Figure 8. (a) UV-Vis spectra of the Methylene blue solutions at stop time 2, 4, 8 and the control sample (b) Comparison of the control sample and the absorbed sample after 8 h.

Conclusion

$\text{Ni}_{0.5}\text{Co}_{0.5}\text{Fe}_2\text{O}_4/\text{AC@Ch}$ nanoparticles were synthesized through co-precipitation and ultrasonic waves and used as a magnetic nanobiocomposite to remove pollutants. Based on BET analysis, the surface area of the nanobiocomposite was $316 \text{ m}^2/\text{g}$. The methylene blue absorption test showed an absorption rate of more than 97% after 8 h. According to the FESEM images, the particle size was about 17 nm, and FTIR and EDAX analysis showed that this compound had a purity of 99% and the reaction was successful. The cubic spinel structure of nickel-cobalt ferrite and the successful coating of chitosan on the surface of the nano-absorbent were confirmed through XRD analysis, and the size of the crystals at the wavelength of 96 nm was obtained through the Bragg equation. FT-IR spectrum of nanoparticles after adsorption confirmed the presence of methylene blue on the nanobiocomposite surface. $\text{Ni}_{0.5}\text{Co}_{0.5}\text{Fe}_2\text{O}_4/\text{AC@Ch}$ can be used as a biocompatible adsorbent due to its large specific surface area and high reactivity, and it is easily removed from aqueous solutions by magnetic separation method.

Data availability

The datasets used and analysed during the current study available from the corresponding author on reasonable request.

Received: 11 November 2022; Accepted: 13 April 2023

Published online: 15 April 2023

References

1. Simonescu, C. M. *et al.* Comparative study of CoFe_2O_4 nanoparticles and CoFe_2O_4 -chitosan composite for Congo red and methyl orange removal by adsorption. *Nanomaterials* **11**(3), 711 (2021).
2. Ouyang, H. *et al.* Fabrication of magnetic cobalt-nickel ferrite nanoparticles for the adsorption of methyl blue in aqueous solutions. *Mater. Res. Express* **8**(10), 105013 (2021).
3. Islam, M. A. *et al.* Removal of dye from polluted water using novel nano manganese oxidebased materials. *J. Water Process Eng.* **10**(9), 32 (2019).
4. Joseph, J., Radhakrishnan, R. C., Johnson, J. K., Joy, S. P. & Thomas, J. Ionexchange mediated removal of cationic dye-stuffs from water using ammonium phosphomolybdate. *Mater. Chem. Phys.* <https://doi.org/10.1016/j.matchemphys.2019.122488> (2019).

5. Lou, T. *et al.* Synthesis of a terpolymer based on chitosan and lignin as an effective flocculant for dye removal. *Colloids Surf. A* **537**, 149–154 (2018).
6. Kim, T. H., Park, C. & Kim, S. Water recycling from desalination and purification process of reactive dye manufacturing industry by combined membrane filtration. *J. Clean. Prod.* **13**, 779–786 (2005).
7. Kumar, P. S. *et al.* Adsorption of dye from aqueous solution by cashew nut shell: Studies on equilibrium isotherm, kinetics and thermodynamics of interactions. *Desalination* **261**, 52–60 (2010).
8. Dafnopatidou, E. K. & Lazaridis, N. K. Dyes removal from simulated and industrial textile effluents by dissolved-air and dispersed-air flotation techniques. *Ind. Eng. Chem. Res.* **47**, 5594–5601 (2008).
9. Wong, P. W., Teng, T. T., Abdul Rahman, N. & Norulaini, N. Efficiency of the coagulation-flocculation method for the treatment of dye mixtures containing disperse and reactive dye. *Water Qual. Res. J.* **42**(1), 54–62 (2007).
10. Gupta, V. K., Agarwal, S., Bharti, A. K. & Sadegh, H. Adsorption mechanism of functionalized multi-walled carbon nanotubes for advanced Cu (II) removal. *J. Mol. Liq.* **230**, 667–673 (2017).
11. Li, Z. *et al.* Adsorption of Congo red and methylene blue dyes on an Ashitaba waste and a walnut shell-based activated carbon from aqueous solutions: Experiments, characterization and physical interpretations. *Chem. Eng. J.* **388**, 124263 (2020).
12. Mahmoodi, N. M. & Saffar-Dastgerdi, M. H. Zeolite nanoparticle as a superior adsorbent with high capacity: Synthesis, surface modification and pollutant adsorption ability from wastewater. *Microchem. J.* **145**, 74–83 (2019).
13. Lei, C., Pi, M., Jiang, C., Cheng, B. & Yu, J. Synthesis of hierarchical porous zinc oxide (ZnO) microspheres with highly efficient adsorption of Congo red. *J. Colloid Interface Sci.* **490**, 242–251 (2017).
14. Konicki, W., Aleksandrak, M., Moszyński, D. & Mijowska, E. Adsorption of anionic azo-dyes from aqueous solutions onto graphene oxide: equilibrium, kinetic and thermodynamic studies. *J. Colloid Interface Sci.* **496**, 188–200 (2017).
15. Salman, D. *et al.* Synthesis, surface modification and characterization of magnetic Fe₃O₄@SiO₂ core-shell nanoparticles. *J. Phys. Conf. Ser.* **1773**(1), 012039 (2021).
16. Briceño, S. *et al.* NiFe₂O₄/activated carbon nanocomposite as magnetic material from petcoke. *J. Magn. Magn. Mater.* **360**, 67–72 (2014).
17. Jadhav, S. A. *et al.* Recent advancements in silica nanoparticles based technologies for removal of dyes from water. *Colloid Interface Sci. Commun.* **30**, 100181 (2019).
18. Mahjoubi, F. Z., Khalidi, A., Abdennouri, M. & Barka, N. Zn–Al layered double hydroxides intercalated with carbonate, nitrate, chloride and sulphate ions: Synthesis, characterisation and dye removal properties. *J. Taibah Univ. Sci.* **11**(1), 90–100 (2017).
19. Ai, L., Zhou, Y. & Jiang, J. Removal of methylene blue from aqueous solution by montmorillonite/CoFe₂O₄ composite with magnetic separation performance. *Desalination* **266**, 72–77 (2011).
20. Fan, L. Preparation of novel magnetic chitosan/graphene oxide composite as effective adsorbents toward methylene blue. *Bioresour. Technol.* **114**, 703–706 (2012).
21. Zhu, H. *et al.* Preparation, characterization and adsorption properties of chitosan modified magnetic graphitized multi-walled carbon nanotubes for highly effective removal of a carcinogenic dye from aqueous solution. *Appl. Surf. Sci.* **285**, 865–873 (2013).
22. Xia, H. *et al.* Adsorption behavior of methylene blue onto waste-derived adsorbent and exhaust gases recycling. *RSC Advances* **7**, 27331–27341 (2017).
23. Reddy, D. H. K. & Lee, S. M. Application of magnetic chitosan composites for the removal of toxic metal and dyes from aqueous solutions. *Adv. Colloid Interface. Sci.* **201**, 68–93 (2013).
24. Li, N. & Bai, R. Highly enhanced adsorption of lead ions on chitosan granules functionalized with poly (acrylic acid). *Ind. Eng. Chem. Res.* **45**(23), 7897–7904 (2006).
25. Ansari, H., Miralinalghi, M. & Azizinezhad, F. CoFe₂O₄/chitosan magnetic nanocomposite: Synthesis, characterization and application for adsorption of acidic yellow dye from aqueous solutions. *Cellul. Chem. Technol.* **53**, 191–204 (2019).
26. Malakootian, M., Nasiri, A. & Mahdizadeh, H. Preparation of CoFe₂O₄/activated carbon@chitosan as a new magnetic nanobio-composite for adsorption of ciprofloxacin in aqueous solutions. *Water Sci. Technol.* **78**(10), 2158–2170 (2018).
27. Jiang, T., Liang, Y. D., He, Y. J. & Wang, Q. Activated carbon/NiFe₂O₄ magnetic composite: A magnetic adsorbent for the adsorption of methyl orange. *J. Environ. Chem. Eng.* **3**(3), 1740–1751 (2015).
28. Guo, X. *et al.* Synthesis of amino functionalized magnetic graphenes composite material and its application to remove Cr (VI), Pb (II), Hg (II), Cd (II) and Ni (II) from contaminated water. *J. Hazard. Mater.* **278**, 211–220 (2014).
29. Asgari, E., Sheikhmohammadi, A. & Yeganeh, J. Application of the Fe₃O₄-chitosan nano-adsorbent for the adsorption of metronidazole from wastewater. Optimization, kinetic, thermodynamic and equilibrium studies. *Int. J. Biol. Macromol.* **164**, 694–706 (2020).

Acknowledgements

I am very grateful to the management of Mir Razi research center for providing the conducting this research.

Author contributions

Z.D. wrote the main manuscript, did experimental part such as preparing chemicals and synthesis nanobio composite with help of Mir Razi research center, reviewed the file containing the nano biocomposite analysis received from Mahamax company. tarjomc site did translate this article.

Competing interests

The author declares no competing interests.

Additional information

Correspondence and requests for materials should be addressed to Z.D.

Reprints and permissions information is available at www.nature.com/reprints.

Publisher's note Springer Nature remains neutral with regard to jurisdictional claims in published maps and institutional affiliations.



Open Access This article is licensed under a Creative Commons Attribution 4.0 International License, which permits use, sharing, adaptation, distribution and reproduction in any medium or format, as long as you give appropriate credit to the original author(s) and the source, provide a link to the Creative Commons licence, and indicate if changes were made. The images or other third party material in this article are included in the article's Creative Commons licence, unless indicated otherwise in a credit line to the material. If material is not included in the article's Creative Commons licence and your intended use is not permitted by statutory regulation or exceeds the permitted use, you will need to obtain permission directly from the copyright holder. To view a copy of this licence, visit <http://creativecommons.org/licenses/by/4.0/>.

© The Author(s) 2023